Finanziato dall'Unione europea NextGenerationEU | Ministero dell'Università e della Ricerca | Italiadomani PIANO NAZIONALE DI RIPRESA E RESILIENZA

multi-Risk sciEnce for resilienT commUnities undeR a changiNg climate Codice progetto MUR: **PE00000005** – H93C22000610002

Deliverable title: Graphs and plots of numerical simulations and laboratory experiments of pyroclastic density currents and Plinian fallout

Deliverable ID:3.3.3

Due date:31/03/2026

Submission date: 31/03/2026

AUTHORS

UNIBA: Pierfrancesco Dellino, Daniela Mele, Fabio Dioguardi, Roberto Sulpizio

1. Technical references

Project Acronym	RETURN
Project Title	multi-Risk sciEnce for resilienT commUnities undeR a changiNg climate
Project Coordinator	Domenico Calcaterra UNIVERSITA DEGLI STUDI DI NAPOLI FEDERICO II domcalca@unina.it
Project Duration	December 2022 – November 2025 (36 months)

Deliverable No.	DV3.3.3
Dissemination level*	
Work Package	WP3.3 - WP Hazard and expected impact of explosive volcanoes
Task	T3.3.3 – Time-space numerical simulation and experiments of the eruptive variables and impact on structures
Lead beneficiary	UNIBA
Contributing beneficiary/ies	UNIBA

* PU = Public

Document history

Version	Date	Lead contributor	Description
0.1	xx.xx.xxxx	First name Last name (Partner short name)	First draft
0.2			Critical review and proofreading
0.3			Edits for approval
1.0			Final version

Finanziato dall'Unione europea NextGenerationEU
Ministero dell'Università e della Ricerca
Italiadomani PIANO NAZIONALE DI RIPRESA E RESILIENZA

2. ABSTRACT

In this deliverable, results of the project activities carried out within the task TK3.3 “Time-space numerical simulation and experiments of the eruptive variables and impact on structures and population” of this project are presented.
The task combined numerical and laboratory experiments to simulate the impact of volcanic hazardous phenomena (tephra fallout, pyroclastic density currents, volcaniclastic debris flows) with currently available models and investigate on their physical properties in order to improve our modelling capabilities. Results were achieved by using newly purchased equipment and establishing collaborations with ongoing projects and partners, also supported by the “Cascade funds”.

Finanziato dall'Unione europea NextGenerationEU | Ministero dell'Università e della Ricerca | Italiadomani PIANO NAZIONALE DI RIPRESA E RESILIENZA

3. Table of contents

List of Tables

List of Figures

Finanziato dall'Unione europea NextGenerationEU | Ministero dell'Università e della Ricerca | Italiadomani PIANO NAZIONALE DI RIPRESA E RESILIENZA

Figure 3. Picture showing the part of the original flume dedicated to the granular flow experiments (on the left) and details of the installation of the gate and opening system constituting the dam-break (centre and right).

Figure 4. Picture showing the preparation of the rough carpet.

Figure 5. Measurements of the experiment with d = 2.6mm, λ/d = 1. a) Normalized flow front propagation over time for different slopes (from bottom to the top, 0°, 10°, 20°, 30°, 36°). b) Flow thickness evolution over time at three positions along the flume. c) Final deposit thickness vs. distance along the flume for four different slopes.

Figure 6. a) Normalized flow front position vs. normalized time for experiments carried out at 10° and 36° slope and three values (0.1, 1, 10) of the λ/d ratio. b) Normalized deposit's thickness vs. normalized distance for experiments at 10° slope and three values (0.1, 1, 10) of the λ/d ratio.

Figure 7. Shear-strength parameters of Soil A versus volumetric water content (VWC, 0–8%) under three pre-shear normal stresses (1, 2 and 3 kPa): (a) mean cohesion, τ_c; (b) mean tensile strength, σ_t; (c) mean unconfined yield strength, σ_c; and (d) mean internal friction angle, φ. Symbols show mean values across replicate tests (n = 3), and error bars indicate ± standard deviation.

Figure 8. Experimental setup and rheological results. a) Anton Paar MCR 703e rheometer. b) Measurement geometries used. c and d) Flow curves for sediment suspensions illustrating Herschel-Bulkley behaviour and geometry-dependent differences in shear stress and apparent viscosity.

4.First Section

4.1 Tephra Fallout modelling

To investigate the impact of tephra fallout, we considered a selected output of tephra load at ground (in kg m^{-2}) taken from a large number of numerical simulations carried out using the open-source Eulerian numerical code FALL3D (v.8.0; Folch et al. 2020), for simulating dispersion of volcanic tephra, gas, and radionuclides, with a wide range of possible model parameterization options (e.g., eruptive parameters, source model, ash aggregation, domain discretization), including the possibility to describe the gravitational spreading of the umbrella region.

4.1 FALL3D model for tephra fallout dispersion

FALL3D is an open-source, three-dimensional, time-dependent Eulerian model designed to simulate the atmospheric transport and deposition of volcanic ash, aerosols, gases, and radionuclides. It operates as an offline transport model, meaning that it is driven by external meteorological data rather than solving the atmospheric dynamics itself. At its core, FALL3D solves the advection–diffusion–sedimentation (ADS) equation, which governs the temporal evolution of the concentration of atmospheric tracers. This equation accounts for three main physical processes:

1) Advection, driven by wind fields, which transports particles horizontally and vertically
2) Turbulent diffusion, parameterized through an eddy diffusivity tensor, representing sub-grid atmospheric mixing
3) Gravitational settling (sedimentation), which controls particle fallout based on size, density, and shape.

The model includes source and sink terms, allowing the specification of emission rates, eruption column characteristics, and removal processes such as deposition or decay.

FALL3D is implemented on a three-dimensional structured grid, typically terrain-following, and uses finite-difference or finite-volume numerical schemes with explicit time integration to solve the governing equations. The model can be run in parallel using domain decomposition, enabling efficient simulations over large spatial domains and long time periods. A key feature of the model is its ability to handle multiple species and particle classes simultaneously, each characterized by specific physical properties (e.g., grain size distribution, density, settling velocity). This allows the simulation of a wide range of atmospheric constituents, including volcanic ash, SO_2, mineral dust, and radionuclides. FALL3D is driven by external meteorological datasets (e.g., reanalysis or forecast models, which provide the time-dependent wind and atmospheric structure fields required for transport calculations.

4.2 Extraction of simulated tephra fallout deposits for RETURNLAND

In Massaro et al. (2023) a long-term tephra fallout hazard assessment in southern Italy posed by the three active Neapolitan volcanoes: Somma–Vesuvius, Campi Flegrei, and Ischia, is proposed. The numerical simulations were run using FALL3D-8.0 (Folch et al. 2020). The meteorological conditions were retrieved from the fifth-generation European Centre for Medium-Range Weather Forecasts global reanalysis dataset (ECMWF ERA5; Hersbach et al., 2023a,b) having a spatial resolution of 0.03° × 0.03° and a temporal resolution of 3 hours, while the volcanic scenario was randomly sampled from a set of eruptive source parameters assessed for the medium-high eruption class of Campi Flegrei as defined in literature (e.g., Martinez

Montesinos et al., 2022; Selva et al., 2022). The simulation output shown in Figure 1 has been translated to the RETURNLAND volcanic vent (red point) showing an eruptive size compatible with the medium-high magnitude eruption class at Campi Flegrei (e.g., Agnano Monte Spina) as defined in literature. The dispersal axis fully covers a selected area (named RV2; see Liso et al., 2026) with potential tephra loads in the range of 600 kg m^{-2} which corresponds to a deposit thickness of ca. 60 cm (assuming a deposit density of ca. 1000 kg m^{-2}).

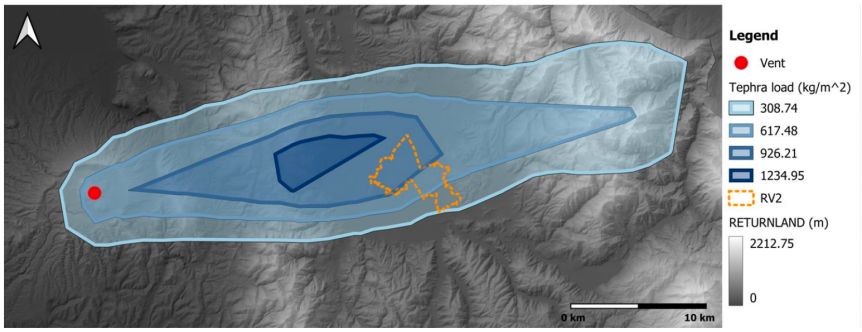

Figure 1. Simulated tephra load (kg m^{-2}) generated using the FALL3D-8.0 model. The red dot marks the location of the eruptive vent, while the dotted orange perimeter indicates the RV2 zone. The background represents the topography of RETURNLAND (in meters), from Liso et al. (2026).

4.2 Numerical simulations of pyroclastic density currents

To investigate the impact of pyroclastic density currents (PDC) generated by eruptive column collapses, we simulated theme on a real topography, including a dock area located about 11 km from the vent. Model calculations were carried out using the ANSYS Fluent simulation tool on a Dell PowerEdge R760XA equipped with two NVIDIA H100 NVL GPUs and connected to a Dell Powerscale A300 storage unit.

4.2.1 Two-Fluid Model in ANSYS Fluent

ANSYS Fluent is a widely used multiphase Computational Fluid Dynamic (CFD) software, which treats multiphase flows simulations with different approaches, e.g. the Discrete Element Method (DEM or Eulerian-Lagrangian) and the Two-Fluid Model (TFM or Eulerian-Eulerian). TFM is more suitable for flows involving large numbers of particles, such as PDCs (Neglia et al., 2023). In the last decades, several authors have successfully applied TFM to volcanic phenomena (e.g., Cerminara et al., 2016; Dartevelle et al., 2004; Dobran et al., 1993; Dufek and Bergantz, 2007; Esposti Ongaro et al., 2008; Neri et al., 2003, 2007; Valentine, 2020; Valentine & Wohletz, 1989). For this reason, TFM was applied to the scenario here investigated. The rectangular computational domain measuring 20 km x 6 km x 7 km in the x (flow direction), y and z dimensions consists of a body-fitted, unstructured hexcore mesh of about 1,000,000. The mesh was developed to accurately resolve the complex topography, especially in regions with steep gradients, without excessive computational cost. Local refinements were applied to the vent, collapsing region, along the main flow path, and around the dock area 11 km from the vent. Cell size in refined zones is set to 50 m, with finer cells of 10 m in the dock area, in order to capture dynamic pressures and flow behavior in detail. The flow inlet corresponds to the volcano summit within the caldera (Fig. 2a). The mass eruption rate (MER) of the inlet is set to 1.6 x 10^8 kg s^{-1}, which falls in the range (10^7 – 10^9 kg s^{-1}) required to

generate PDCs (Cioni et al., 2000). The solid phase at the inlet has density of 1550 kg m^{-3}, mean particle size of 25 µm, and temperature of 800 °C.

Figure 2 shows the velocity magnitude of PDCs generated by column collapse on the reconstructed topography, with the vertical profile of dynamic pressure in the dock area. Generally, PDCs spread radially from the impact zone (dashed line, Fig. 2a) toward the domain boundaries, along the main ravines. The impact zone is recognizable by a central area of low velocities, which denote the granular compaction phase. In this stage, the gas pressure increases, forcing lateral expansion of the mixture. The maximum simulated velocities about 150 m s^{-1} are reached in the downstream zone adjacent to the impact area, where PDCs bypass the morphological highs before being channelized in the main ravines, reaching velocities of 70 – 100 m s^{-1}. Near the dock area (highlighted in Fig. 2a), the velocities drop to 40 – 50 m s^{-1}. Figure 2b shows a *yz*-plane slice of ash velocity magnitude, including a portion of the flow impacting. In this area, the flow has a thickness of about 200 m, with maximum velocities of 52 m s^{-1}. A second pulse can be seen following the main flow inundating the dock area. The presence of multiple pulses has been observed during large- and small-scale laboratory experiments (e.g., Iverson, 1997; Savage & Hutter, 1989) and hypothesized for both volcaniclastic and pyroclastic deposits based on field evidence (e.g., Chough and Sohn, 1990; Sulpizio et al., 2007; Sulpizio and Dellino, 2008). The arrival of different PDCs in the inundated areas concurs to the final hazard. Figure 2c reports a zoom of the dock area, showing the flow passage over the concave-downward slope near the dock. This passage is characterized by a hydraulic jump of the flow, which decreases its velocity and increases its thickness (from supercritical to subcritical flow). Figure 2d-f shows the vertical profile of dynamic pressures (P_{dyn}), temperatures (T) and concentrations (c) in the same area. Despite the 11 km of travelled distance from the vent to inhabited area, over complex terrain, the PDC retains dynamic pressures of 3.3 kPa at 10 m above the ground, with solid concentration of $5x10^{-4}$ and temperature of 600 °C. These values are consistent with previous studies (Baxter et al., 1998; Dellino et al., 2008; Valentine, 1998) and suggest potential damage to building openings, causing the ingress of hot ashes into structures. This increases the amount of damage and poses serious risks to human health. In this case, the mechanical effects of the currents on buildings are secondary to impact of high temperatures (> 500 °C) and ash concentrations, which are exacerbated by the prolonged exposure time (several minutes) during the flow passage. Furthermore, these dynamic pressures can flatten up to 90 % of trees (Glasstone and Dolan, 1977), making the area impassable to vehicles and severely hindering the emergency services.

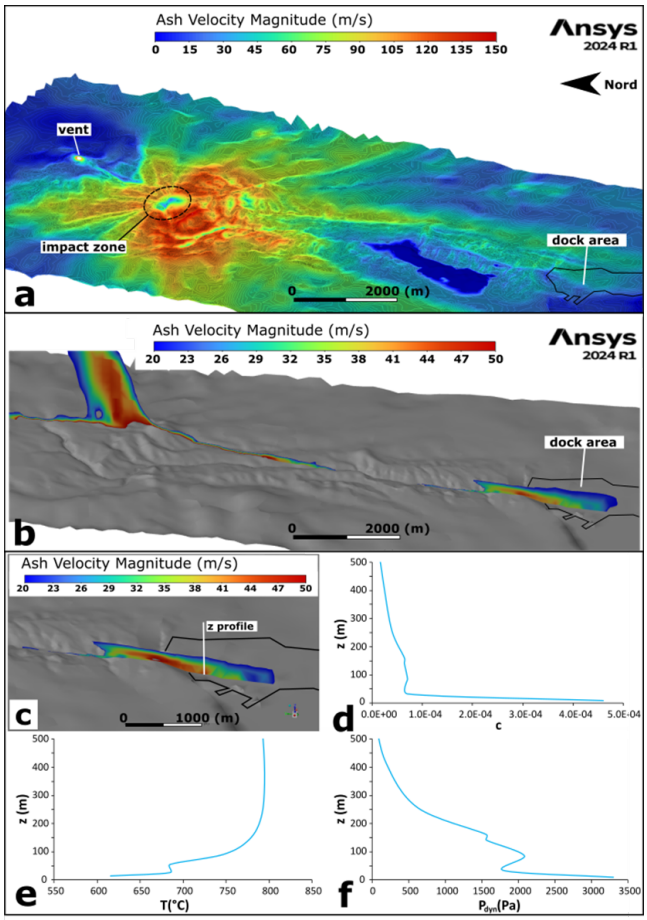

Figure 2. a) Contour map of ash velocity magnitude at ground level, b) ash velocity magnitude along a vertical yz-slice, c) zoomed view of ash velocity contour in the dock area, vertical profile of (d) ash concentration, (e) temperature, and (f) dynamic pressure.

4.3 Large-scale experiments on the transportation dynamics of granular flows

In cooperation with the PRIN 2022 PNRR project P2022CLRTF 'Improving the modeling capabilities of geophysical granular flows through experimental and numerical simulations', we carried out large-scale experiments on the propagation dynamics of dry granular flows as a proxy of dense pyroclastic density currents. The main purpose of the experiments was to investigate the influence of the basal roughness on the granular flow propagation and deposition.

4.3.1 Experimental setup

The experiments were carried out in a flume that was already available at the CamiLab of the University of Calabria (Fig. 3). The flume, originally dedicated to rainfall-triggering of debris flows, was adapted to reproduce granular flows fed by a dam break. Specifically, the final adapted flume is 6 m long, 0.5 m wide.

Figure 3. Picture showing the part of the original flume dedicated to the granular flow experiments (on the left) and details of the installation of the gate and opening system constituting the dam-break (centre and right).

The new dam-break release was constructed to feed a flow of up to 0.35 m3 of granular material. The system was obtained by installing a manually-driven 0.5 m-wide and 1 m-high sliding gate that separate the uppermost part of the flume (1 m-long, 0.5 m-wide) and guarantees an opening up to 0.75 m. Fig. 1 shows the details of the dam-break installation.

The employed granular material consisted of sediments (construction materials) of various sizes, ranging from fine sand to gravel. The basal roughness was achieved by gluing sediment particles from the same batch used in the flow experiments on rubber carpets (Fig. 4).

Figure 4. Picture showing the preparation of the rough carpet.

In the experimental campaign, we conducted experiments by varying:

- The channel slope θ;
- The particle mean grainsize d;
- The roughness λ, measured by means of a Leica electronic stereomicroscope installed at the University of Bari.

Details of the parameters of the experiments are shown in Table 1.

Table 1 - List of parameters of the large-scale experiments. *H* is the initial granular material column height, ϑr; is the repose angle of the granular material.

Test #	m (kg)	H (m)	d (m)	λ (m)	λ/d	θ_r	θ [°]
1	361.3	0.506	0.0026	0.00239	0.919	33.3	0.0
2	361.5	0.513	0.0026	0.00239	0.919	33.3	10.0
3	361.5	0.498	0.0026	0.00239	0.919	33.3	20.0
4	361.5	0.501	0.0026	0.00239	0.919	33.3	30.0
5	361.5	0.501	0.0026	0.00239	0.919	33.3	36.0
6	368.8	0.503	0.00027	0.00239	8.852	32.2	0.0
7	368.8	0.523	0.00027	0.00239	8.852	32.2	10.0
8	368.8	0.501	0.00027	0.00239	8.852	32.2	20.0
9	368.8	0.503	0.00027	0.00239	8.852	32.2	30.0
10	368.8	0.501	0.00027	0.00239	8.852	32.2	36.0
11	361.5	0.496	0.0026	0.00239	0.919	33.3	30.0
12	361.5	0.496	0.0026	0.00239	0.919	33.3	30.0
13	368.8	0.496	0.00027	0.00027	1.000	32.2	10.0
14	368.8	0.506	0.00027	0.00027	1.000	32.2	0.0
15	368.8	0.504	0.00027	0.00027	1.000	32.2	20.0
16	368.8	0.504	0.00027	0.00027	1.000	32.2	30.0
17	368.8	0.500	0.00027	0.00027	1.000	32.2	36.5
18	361.5	0.490	0.0026	0.00027	0.104	33.3	0.0
19	361.5	0.500	0.0026	0.00027	0.104	33.3	20.0
20	361.5	0.495	0.0026	0.00027	0.104	33.3	10.0
21	361.5	0.495	0.0026	0.00027	0.104	33.3	30.0
22	361.5	0.498	0.0026	0.00027	0.104	33.3	36.0
23	368.8	0.503	0.00027	0.00027	1.000	32.2	30.0
24	401.1	0.493	0.00087	0.00027	0.310	34.3	20.0

4.3.2 Results

By means of ultrasonic and laser distance-metres, we monitored the spatial and temporal evolution of the flow propagation and thickness. Figure 4 shows an example (experiment with (d = 2.6mm, λ/d = 1), of monitored flow front (position x from the flow inlet normalized by the initial deposit length L0) propagation over time (Fig. 5a), flow thickness (normalized by the initial deposit height H0) evolution over time at various locations downstream (Fig. 5b) and the thickness of the final deposit for various slopes (Fig. 5c).

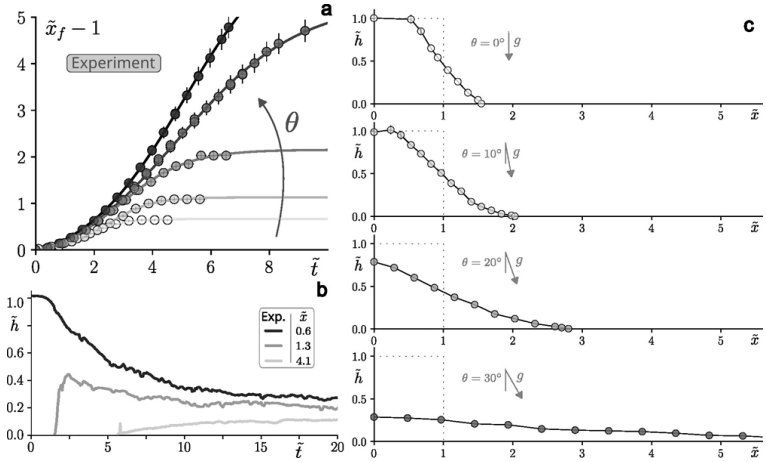

Figure 5. Measurements of the experiment with d = 2.6mm, λ/d = 1. a) Normalized flow front propagation over time for different slopes (from bottom to the top, 0°, 10°, 20°, 30°, 36°). b) Flow thickness evolution over time at three positions along the flume. c) Final deposit thickness vs. distance along the flume for four different slopes.

The main finding of these experiments is that both the flow propagation dynamics and the final deposit do not show any dependency on the basal condition, quantified by the λ/d ratio. This is evident in Fig. 6, where the flow front propagation vs. time and the deposit's thickness vs. distance for two slopes and three different values of the λ/d ratio are represented.

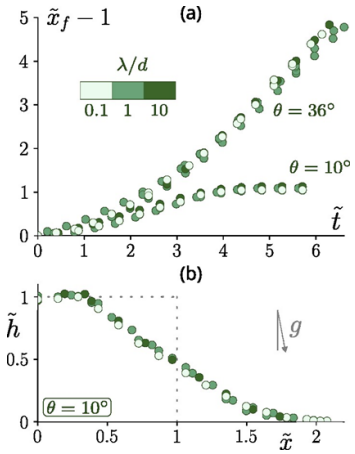

Figure 6. a) Normalized flow front position vs. normalized time for experiments carried out at 10° and 36° slope and three values (0.1, 1, 10) of the λ/d ratio. b) Normalized deposit's thickness vs. normalized distance for experiments at 10° slope and three values (0.1, 1, 10) of the λ/d ratio.

This behaviour can be attributed to the fact that, in a dam-break configuration, in which the granular material starts moving from rest and propagates as the result of gravitational forces, the inertial forces play a minor role. The rheology of the granular flows, which controls also the basal friction, strongly depend on the particle inertial number, which is relatively small in the reproduced flows. This finding, corroborated by numerical simulations carried out within the PRIN 2022 PNRR P2022CLRTF project, can have interesting implications for natural granular flows like, e.g., small debris avalanches fed by dome collapses. The experiments, together with numerical models, seem to indicate that, when simulating flows in these regimes, one may focus on parameters like the initial thickness, initial volume and slope. For example, the experimental trend fits satisfactorily with the Ln vs. θ scaling laws of Mangeney et al. (2010) and Bougouin et al. (2026), where Ln is the final normalized runout of the flow.

4.4. Laboratory experiments on the rheology of volcaniclastic materials

In this section we present results of laboratory rheological measurements on volcanic materials carried out to characterize the triggering and propagation factors of volcaniclastic debris flows.

4.4.1 Triggering factors of volcaniclastic debris flows: the influence of soil humidity.

Volcaniclastic debris flows can initiate rapidly and develop high velocities and destructive power, making their prediction and mitigation strongly dependent on an accurate description of the mechanical behavior of the source materials. This study quantifies how small, progressive increases in volumetric water content (VWC) modify the shear-failure response of ash-rich soils from the Sarno area (Campanian Volcanic Province, Southern Italy), which was the site of catastrophic flows that, on the 5-6 May 2008 killed 161 people. Three representative ash-dominated layers (Soils A, C, and E) were investigated under controlled laboratory conditions by coupling basic material characterization with a systematic shear-to-failure testing program. Moisture was increased from dry conditions to 8% VWC in 2% steps, and undrained shear experiments were performed to reconstruct yield loci and derive strength-related parameters (Pace et al., 2026).

4.4.1.1 Methodology

The samples were first characterized to constrain the physical and compositional properties known to influence the mechanical response of ash-rich granular materials; i.e., particle-size distribution, skeletal density, and mineralogical composition were determined on dried subsamples. The shear-failure response was therefore investigated through controlled powder-shear tests. Specifically, shear-failure measurements were conducted using an Anton Paar MCR 702e MultiDrive rheometer equipped with an Anton Paar Powder Shear Cell (PSC43-21-12) and the corresponding lower shaft. Environmental conditions were controlled using a CTD 180 HR device coupled with an MHG 100 humidity generator, allowing tests to be carried out under fixed temperature and relative humidity. All measurements were performed at 27 °C and 50% Relative Humidity (RH) to limit sensitivity to ambient fluctuations and improve reproducibility. Data acquisition and processing were handled within Anton Paar RheoCompass™ software.

The fine fraction (<500 µm) of the ash-rich soils (A, C and E) was selected for shear-cell testing due to cell-geometry and operational constraints, ensuring stable packing and reproducible shearing within the vessel. Tests were performed on oven-dried material (≥72 h at >60 °C; near-zero-moisture reference) and on specimens wetted to target VWC values of 2%, 4%, 6% and 8% by adding distilled water, followed by careful homogenization and disaggregation of agglomerates. The powder was gently loaded into the vessel (in excess to minimize pre-compaction and air inclusions), levelled and weighed to determine bulk density, and

then conditioned under controlled temperature/humidity. Each test included (i) an initial pre-compaction to standardize the starting state, (ii) a pre-shear stage at constant normal stress until a steady-state is reached, and (iii) a series of shear-to-failure steps at reduced normal stresses to extract peak shear stresses for yield-locus construction.

Three pre-shear normal stresses were applied (1, 2, and 3 kPa). For each level, shear-to-failure was performed at three reduced normal stresses (1 kPa: 0.4, 0.6, 0.8 kPa; 2 kPa: 0.8, 1.2, 1.6 kPa; 3 kPa: 1.2, 1.8, 2.4 kPa), at a constant rotational speed of 0.05 rpm. The steady-state tolerance in the software was set to 0.8%, with defined averaging windows and inspection intervals to determine convergence. Yield loci were reconstructed in the σ–τ space through least-squares linear regression of the three yield points obtained for each pre-shear condition. From these loci, the study derived strength-related parameters including cohesion τ_c, tensile strength σ_t, unconfined yield strength σ_c, and an effective friction angle φ. For each combination of soil, moisture level, and pre-shear stress, three independent tests were performed (n = 3), and mean values and standard deviations were obtained. The flow function coefficient was computed from mean-based values and associated uncertainty was estimated by standard propagation for a ratio.

4.4.1.2 Results and Discussion

Across all three soils, increasing VWC produces systematic changes in derived shear-failure parameters, although the details differ by material and confinement level. The progressive wetting within the investigated range (0–8% VWC) produced a consistent reorganization of the shear-failure response of the ash-rich soils, shifting the behaviour from predominantly frictional and easy flowing at low moisture toward increasingly cohesive and tensile-resisting at higher VWC. Across the dataset, cohesion and unconfined yield strength generally increased with water content-most clearly at 6-8% VWC-whereas the friction angle tended to decrease toward the wettest condition, indicating a progressive reduction of the purely frictional contribution as moisture-driven bonding becomes more influential. Tensile strength evolved accordingly, typically becoming more negative at higher VWC, and the associated scatter increased near 8% VWC, consistent with the greater sensitivity of wet specimens to small heterogeneities in water distribution and to the undrained testing configuration.

XRPD analyses did not reveal the presence of clay minerals, supporting the interpretation that the observed water sensitivity is not governed by clay-related mechanisms but is consistent with moisture-enhanced interparticle bonding in granular ash powders.

As a representative example, Figure 7 displays the moisture-dependent response of Soil A (selected parameters shown as a function of VWC), illustrating the progressive increase in cohesive contribution and the concurrent reduction in frictional component.

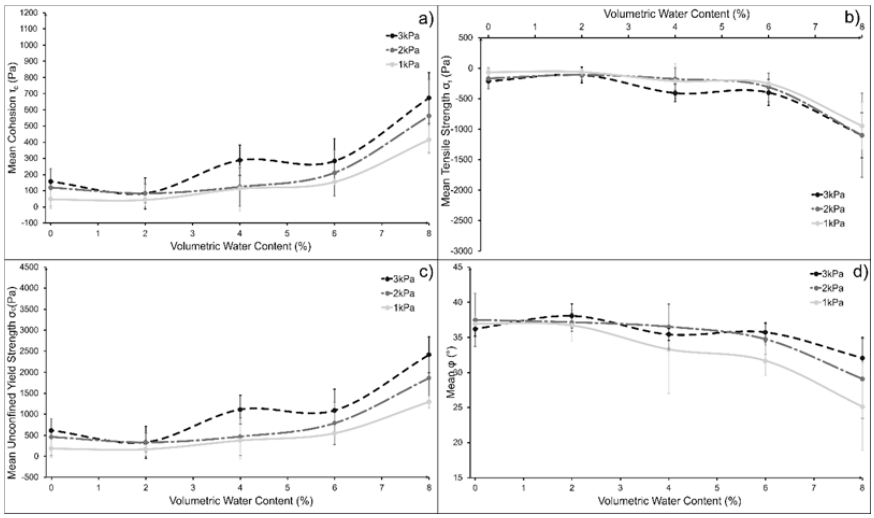

Figure 7. Shear-strength parameters of Soil A versus volumetric water content (VWC, 0–8%) under three pre-shear normal stresses (1, 2 and 3 kPa): (a) mean cohesion, τ_c; (b) mean tensile strength, σ_t; (c) mean unconfined yield strength, σ_c; and (d) mean internal friction angle, ϕ. Symbols show mean values across replicate tests (n = 3), and error bars indicate ± standard deviation.

4.4.2 Rheology of volcaniclastic slurries

Studying the rheological behaviour of sediment suspensions is fundamental for understanding the physical processes governing particle-fluid interactions in lahars. The interstitial fluid in these flows consists of fine sediment suspensions that occupy the pore spaces between larger clasts. This fluid strongly influences flow dynamics by controlling consistency, velocity, and the transport and deposition of coarse particles (Vallance and Iverson, 2015).

Although several theoretical models have been proposed to describe the rheology of fine sediment suspensions, such as Bingham, Herschel-Bulkley, and Dual-Bingham models (Jeong, 2010; Schatzmann et al., 2003), their applicability depends on key material properties, including volumetric sediment concentration, grain-size distribution, particle density, shape, and composition (Vallance, 2000). These variables also constrain the selection of appropriate measurement techniques and experimental scale.

This project (Tranquilino et al., 2026) was developed using the Anton Paar MCR 703e rheometer (Fig. 8a), a rotational rheometer designed to measure the response of liquids and semi-solid materials to controlled deformation. In this device, the sample is placed between a fixed cup and a rotational tool, allowing controlled shear rate tests. Different rotor geometries were employed, including absolute Concentric Cylinder and relative Vane configurations (Fig. 8b), selected according to suspension properties and measurement objectives. These geometries operate under the principle that viscous materials resist relative motion between layers when subjected to shear stress. By systematically varying the angular velocity of the rotor, shear stress responses were recorded, enabling the calculation of apparent viscosity and the identification of rheological models.

A down-rate Staircase protocol was proposed over a shear rate range from 10^2 to 10^{-2} s^{-1}, with 50-second measurement intervals and pre-shearing steps of 30 s at 10^3 s^{-1}. The duration of each interval was determined analytically by calculating particle drag coefficient and terminal settling velocities following Dioguardi et al. (2018). This approach ensured laminar, steady-state flow conditions and minimized sedimentation effects within the suspension.

Sediment suspensions with volumetric particle concentrations between 45 to 60 % were analysed, encompassing conditions representative of mudflow-like interstitial fluid in natural lahars. The results indicate that the suspensions predominantly exhibit Herschel-Bulkley behaviour (Fig. 8c and d), with yield strength values ranging from 10^{-2} to 10^1 Pa within a shear rate range of 1 to 10^{-2} s-1. Furthermore, at higher shear rates, between 1 and 10^2 s^{-1} an increase in recorded shear stress was observed, influencing the decrease in apparent viscosity at high deformation rates. Consequently, the characterized sediment suspensions displayed an apparent viscosity dependent on shear rate, exhibiting shear thinning behaviour at high shear rates and shear thickening behaviour at low shear rates.

The study revealed comparable patterns in the rheological data obtained using the relative Vane geometry and a scale factor one order of magnitude higher, facilitating comparison with data obtained through the absolute geometries. However, the apparent viscosity exhibited a linear relationship with the shear rate, which made it more difficult to identify a possible change in rheological behaviour using this type of tool. The characterized sediment suspensions displayed shear thinning behaviour throughout the entire range of shear rates studied.

Additionally, the volumetric concentration was reflected in shear stress differences of up to two orders of magnitude within the tested sediment concentration range for the absolute Concentric Cylinder geometry (Fig. 8c). An increase in shear stress values was observed for suspensions with higher sediment content. In contrast, for the relative Vane geometry, the difference in shear stress values was three orders of magnitude (Fig. 8d). This highlights the importance of geometry selection in the characterization of sediment suspensions and suggests data scaling.

Finanziato dall'Unione europea NextGenerationEU
Ministero dell'Università e della Ricerca
Italiadomani PIANO NAZIONALE DI RIPRESA E RESILIENZA

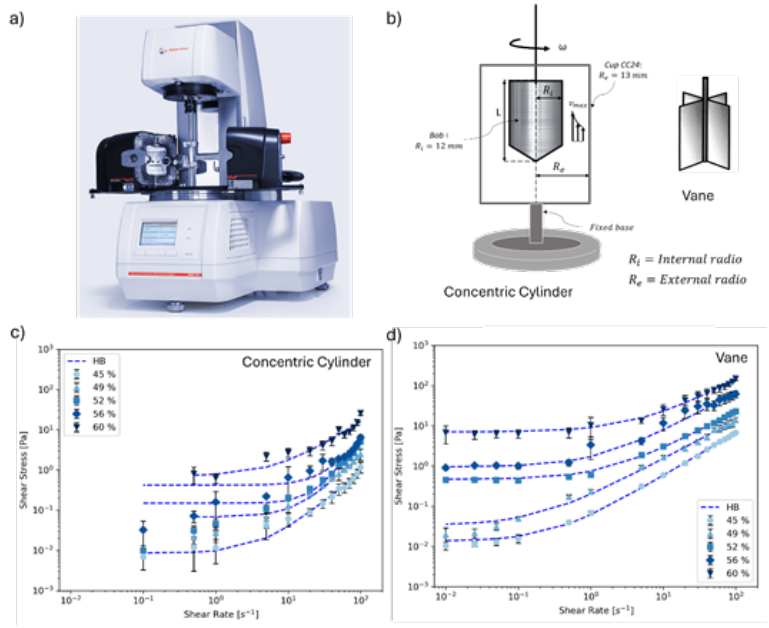

Figure 8. Experimental setup and rheological results. a) Anton Paar MCR 703e rheometer. b) Measurement geometries used. c and d) Flow curves for sediment suspensions illustrating Herschel-Bulkley behaviour and geometry-dependent differences in shear stress and apparent viscosity.

5. Conclusions

In this deliverable we summarized some of the scientific achievements reached in the task TK3.3 "Time-space numerical simulation and experiments of the eruptive variables and impact on structures and population" of this project. Most of the results were obtained working on equipment and instrumentation purchased within this project, namely:

- Dell PowerEdge R760XA equipped with two NVIDIA H100 NVL GPUs and connected to a Dell Powerscale A300 storage unit;
- Anton Paar MCR 702e MultiDrive rheometer equipped with:
    - an Anton Paar Powder Shear Cell;
    - a Concentric Cylinder and a Vane geometries.

We conducted probabilistic volcanic tephra and fallout simulations for eruptive scenarios both at the Campanian volcanoes (Campi Flegrei, Vesuvius and Ischia) and the RETURNLAND volcano, providing maps of static loads at different exceedance probabilities.

By means of state-of-the-art CFD tools on High Performance Computing resources, we simulated the impact of pyroclastic density currents generated during scenario simulations at the RETURNLAND volcano. Specifically, we defined maps and profiles of the flow velocities, temperature, particle volumetric concentrations and dynamic pressure, taking into account the interaction with the terrain at high resolution.

In order to better understand the behavior of granular mixtures that characterize pyroclastic density currents, we conducted large-scale experiments on the propagation dynamics of granular flows. The experiments focused on the interaction between the flow and the substrate, varying the particle-to-roughness ratios. Results of the first experimental campaign showed that there is no clear effect of the substrate roughness on the flow deposition in unsteady dam-break-generated avalanches, which can be considered as proxies of natural flows like short-lived debris avalanches or pyroclastic density currents generated by lava dome failure.

Finally, we conducted laboratory analyses on the rheology of volcaniclastic materials in order to characterize the effect of increasing soil moisture on the stability of volcanic soils and the rheology of volcaniclastic debris flows. We found that, at low moisture levels, the cohesion, unconfined yield strength and tensile strength increases at increasing water content, which implies that soils increases their stability at increasing soil moisture when the latter is low. When analysing the rheology of water-particles mixtures, we observed a shear thinning behaviour of all the analysed mixtures at increasing particle volumetric fraction, whose effect was limited to the increase of apparent viscosity at increasing particle volumetric fraction.

Future work will extend the range of applications of all the instruments and methodologies tested during the project RETURN. We will test upgraded versions of the numerical models for pyroclastic density currents, including temporally-evolving high-resolution terrain models capable of capturing the potential collapses of buildings due to the impact of the currents during the simulation. New large-scale experiments at the CamiLab of Unviversity of Calabria are already planned, exploring different ranges of particle flow rates reaching long-lived steady state releases at controlled flow thickness thanks to the new capabilities developed as the result of the Bando a Cascata. The rheology of volcaniclastic mixtures will continue to be investigated, including dry mixtures at different degrees of fluidization, in order to extend the range of application to pyroclastic density currents.

Commentato [FD1]: Qui citerei il bando a cascata calabrese, ma non conosco i dettagli né come dovrei citarlo

6. References

Baxter, P. J., Neri, A., & Todesco, M. (1998). Physical modelling and human survival in pyroclastic flows. *Natural Hazards*, *17*(2), 163–176. https://doi.org/10.1023/A:1008031004183/METRICS

Bougouin A, Dioguardi F, Capparelli G, et al (2026b) A multi-purpose largescale laboratory flume for gravity driven flows. P-LRT 5(1)

Cerminara, M., Esposti Ongaro, T., & Neri, A. (2016). Large Eddy Simulation of gas–particle kinematic decoupling and turbulent entrainment in volcanic plumes. *Journal of Volcanology and Geothermal Research*, *326*, 143–171. https://doi.org/10.1016/J.JVOLGEORES.2016.06.018

Chough, S. K., & Sohn, Y. K. (1990). Depositional mechanics and sequences of base surges, Songaksan tuff ring, Cheju Island, Korea. *Sedimentology*, *37*(6), 1115–1135. https://doi.org/10.1111/J.1365-3091.1990.TB01849.X;JOURNAL:JOURNAL:13653091;REQUESTEDJOURNAL:JOURNAL:13653091;WGROUP:STRING:PUBLICATION

Cioni, R., Levi, S., & Sulpizio, R. (2000). Apulian Bronze Age pottery as a long-distance indicator of the Avellino Pumice eruption (Vesuvius, Italy).

Dartevelle, S., Rose, W. I., Stix, J., Kelfoun, K., & Vallance, J. W. (2004). Numerical modeling of geophysical granular flows: 2. Computer simulations of plinian clouds and pyroclastic flows and surges. *Geochemistry, Geophysics, Geosystems*, *5*(8), 8004. https://doi.org/10.1029/2003GC000637

Dellino, P., Mele, D., Sulpizio, R., Volpe, L. La, & Braia, G. (2008). A method for the calculation of the impact parameters of dilute pyroclastic density currents based on deposit particle characteristics. *Journal of Geophysical Research: Solid Earth*, *113*(B7).

Dioguardi, F., Mele, D., Dellino, P., 2018. A New One-Equation Model of Fluid Drag for Irregularly Shaped Particles Valid Over a Wide Range of Reynolds Number. J. Geophys. Res.: Solid Earth., v. 123, 144-156.

Dobran, F., Neri, A., & Macedonio, G. (1993). Numerical simulation of collapsing volcanic columns. *Journal of Geophysical Research*, *98*(B3), 4231–4259.

Dufek, J., & Bergantz, G. W. (2007). Suspended load and bed-load transport of particle-laden gravity currents: The role of particle-bed interaction. *Theoretical and Computational Fluid Dynamics*, *21*(2), 119–145. https://doi.org/10.1007/S00162-007-0041-6/METRICS

Esposti Ongaro, T., Neri, A., Menconi, G., de'Michieli Vitturi, M., Marianelli, P., Cavazzoni, C., Erbacci, G., & Baxter, P. J. (2008). Transient 3D numerical simulations of column collapse and pyroclastic density current scenarios at Vesuvius. *Journal of Volcanology and Geothermal Research*, *178*(3), 378–396. https://doi.org/10.1016/J.JVOLGEORES.2008.06.036

Folch, A., Mingari, L., Gutierrez, N., Hanzich, M., Macedonio, G., Costa, A. (2020). FALL3D-8.0: a computational model for atmospheric transport and deposition of particles, aerosols and radionuclides–Part 1: Model physics and numerics. *Geoscientific Model Development*, *13*(3), 1431 - 1458.

Glasstone, S., Dolan, P.J., 1977. The effects of nuclear weapons. US Dept. of Defense and Dept. of Energy, 653 pp.

Hersbach, H., Bell, B., Berrisford, P., Biavati, G., Horányi, A., Muñoz Sabater, J., Nicolas, J., Peubey, C., Radu, R., Rozum, I., Schepers, D., Simmons, A., Soci, C., Dee, D., Thépaut, J-N. (2023a). ERA5 hourly data on single levels from 1940 to present. Copernicus Climate Change Service (C3S) Climate Data Store (CDS), DOI: 10.24381/cds.adbb2d47 (Accessed on 14-02-2026).

Hersbach, H., Bell, B., Berrisford, P., Biavati, G., Horányi, A., Muñoz Sabater, J., Nicolas, J., Peubey, C., Radu, R., Rozum, I., Schepers, D., Simmons, A., Soci, C., Dee, D., Thépaut, J-N. (2023b). ERA5 hourly data on pressure levels from 1940 to present. Copernicus Climate Change Service (C3S) Climate Data Store (CDS), DOI: 10.24381/cds.bd0915c6 (Accessed on 14-02-2026).

Iverson, R. M. (1997). The Physics of Debris Flows. *Reviews of Geophysics*, *35*(3), 245–296. https://doi.org/10.1029/97RG00426;

Jeong, S., 2010. Grain size dependent rheology on the mobility of debris flows. Geosci. J., v. 14(4), 359-369.

Liso, I.S., Tufano, R., Poneti, G., Scacchia, E., Colacicco, R., Lo Presti, V., Bausilio, G., Massaro, S., Neglia, F., Scardino, G., Zaniboni, F., Di Napoli, M., Laurenti, A., Calcaterra, D., Ceramicola, S., Chiocci, F.L., Dellino, P., Parise, M.m Sulli, A. Martino, S. (2026). Design of a Virtual Test Bed for the Italian territory: Proof of Concept for Multi-hazard scenarios effects in the context of a national resilience assessment. *International Journal of Disaster Risk Reduction*, *under review*.

Mangeney A, Heinrich P, Roche R (2000) Analytical solution for testing debris avalanche numerical models. Pure Appl Geophys 157(6):1081–1096

Martinéz Montesinos, B., Titos Luzón, M., Sandri, L., Oleksandr, R., Cheptov, A., Macedonio, G., Folch, A., Barsotti, S., Selva, J., and Costa, A. (2022). On the feasibility and usefulness of high-performance computing in probabilistic volcanic hazard assessment: An application to tephra hazard from Campi Flegrei, *Frontiers in Earth Sciences*, 1–26, https://doi.org/10.3389/feart.2022.941789 .

Massaro, S., Stocchi, M., Martínez Montesinos, B., Sandri, L., Selva, J., Sulpizio, R., Giaccio, B., Moscatelli, M., Peronace, E., Nocentini, M., Isaia, R., Titos Luzón, M., Dellino, P., Naso, G., and Costa, A. (2023). Assessing long-term tephra fallout hazard in southern Italy from Neapolitan volcanoes, Nat. Hazards Earth Syst. Sci., 23, 2289–2311, https://doi.org/10.5194/nhess-23-2289-2023.

Neri, A., Esposti Ongaro, T., Macedonio, G., & Gidaspow, D. (2003). Multiparticle simulation of collapsing volcanic columns and pyroclastic flow. *Journal of Geophysical Research: Solid Earth*, *108*(B4), 2202. https://doi.org/10.1029/2001JB000508;CTYPE:STRING:JOURNAL

Neri, A., Ongaro, T. E., Menconi, G., De', M., Vitturi, M., Cavazzoni, C., Erbacci, G., Baxter, P. J., Ongaro, E., Menconi, G., De', M., Cavazzoni, C., Erbacci, G., & Baxter, P. J. (2007). 4D simulation of explosive eruption dynamics at Vesuvius. *Geophysical Research Letters*, *34*(4), 4309. https://doi.org/10.1029/2006GL028597

Pace, L., Dioguardi, F., Gentile, L., Lacalamita, M., Capparelli, G., Sulpizio, R., Dellino, P., 2026. Volumetric Water Content and Shear Failure of Volcanic Ash: Evidences from Powder Shear Cell Analyses. Environ. Eng. Geosci., *under review*.

Savage, S. B., & Hutter, K. (1989). The motion of a finite mass of granular material down a rough incline. *Journal of Fluid Mechanics*, *199*(2697), 177–215. https://doi.org/10.1017/S0022112089000340

Schatzmann, M., Fischer, P., Bezzola, G., 2003. Rheological behavior of fine and large particle suspensions. J. Hydraul. Eng. ASCE., v. 129(10), 796-803.

Selva, J., Sandri, L., Taroni, M., Sulpizio, R., Tierz, P., and Costa, A. (2022). A simple two-state model interprets temporal modulations in eruptive activity and enhances multi-volcano hazard quantification, Sci. Adv., 8, 8.44, eabq4415, https://doi.org/10.1126/sciadv.abq4415.

Sulpizio, R., & Dellino, P. (2008). Chapter 2 Sedimentology, Depositional Mechanisms and Pulsating Behaviour of Pyroclastic Density Currents. *Developments in Volcanology*, *10*(C), 57–96. https://doi.org/10.1016/S1871-644X(07)00002-2

Sulpizio, R., Mele, D., Dellino, P., & La Volpe, L. (2007). Deposits and physical properties of pyroclastic density currents during complex Subplinian eruptions: The AD 472 (Pollena) eruption of Somma-Vesuvius, Italy. *Sedimentology*, *54*(3), 607–635. https://doi.org/10.1111/J.1365-3091.2006.00852.X;WGROUP:STRING:PUBLICATION

Tranquilino, C., Dioguardi, F., Gentile, L., Dellino, P., Caballero, L., Sarocchi, D., Lacalamita, M. (2026). An experimental method for measuring the rheological behavior of slurry suspensions. *Applied Rheology*, *under review*.

Valentine, G. A. (1998). Damage to structures by pyroclastic flows and surges, inferred from nuclear weapons effects. *Journal of Volcanology and Geothermal Research*, *87*(1–4), 117–140. https://doi.org/10.1016/S0377-0273(98)00094-8

Valentine, G. A. (2020). Initiation of dilute and concentrated pyroclastic currents from collapsing mixtures and origin of their proximal deposits. *Bulletin of Volcanology*, *82*(2). https://doi.org/10.1007/s00445-020-1366-x

Valentine, G. A., & Wohletz, K. H. (1989). Numerical models of Plinian eruption columns and pyroclastic flows. *Journal of Geophysical Research*, *94*(B2), 1867–1887. https://doi.org/10.1029/JB094IB02P01867

Vallance, J. W., 2000. Lahars. In Sigurdsson, H. (Ed.), Encyclopedia of Volcanoes (1st ed., pp. 601-615) Academic Press, San Diego.

Vallance, J. W., and Iverson, R., 2015. Lahars and their deposits. In Sigurdsson, H. (Ed.), Encyclopedia of Volcanoes (2nd ed., pp. 649-664). Academic Press, San Diego.